

## Design of Experiments (DOE) for the Optimization of Hydrothermal Synthesis of Hydroxyapatite Nanoparticles

Mehdi Sadat-Shojai,\* Mohammad Atai and Azizollah Nodehi

Iran Polymer and Petrochemical Institute, P.O. Box 14965-115 Tehran, Iran

O objetivo deste trabalho foi investigar a influência de diversos parâmetros de reação sobre as propriedades de nanopartículas de hidroxiapatita (HAp) preparadas pelo método hidrotérmico. Os dados da literatura descrevem condições experimentais variadas para a síntese hidrotérmica de HAp. Uma abordagem específica foi então utilizada para avaliar os fatores estatisticamente influentes entre aqueles descritos na literatura. O papel de cada parâmetro experimental também foi discutido no contexto da nucleação de partículas e do mecanismo de crescimento de cristais. Dentro das variáveis selecionadas, temperatura e pH foram os fatores que mais afetaram a composição e morfologia da HAp. Além disso, neste estudo, diferentes morfologias variando de nanopartículas cilíndricas do tipo bastonete a esféricas com várias características foram obtidas com sucesso, o que pode ser aplicável na preparação de várias biocerâmicas de HAp.

The aim of this work was to investigate the influence of different reaction parameters on the properties of hydroxyapatite (HAp) nanoparticles prepared by the hydrothermal method. The literature data describe widely different experimental conditions for the hydrothermal synthesis of HAp. A specific approach was therefore used to evaluate the statistically influential factors among those described in the literature. The role of each experimental parameter was also discussed within the framework of particle nucleation and crystal growth mechanism. Among the selected variables, temperature and pH were found to be the most significant factors affecting the composition and morphology of the HAp. Moreover, in the present study, different morphologies ranging from rod-like to spherical nanoparticles with various characteristics were successfully obtained, which can be applicable for the preparation of various HAp bioceramics.

**Keywords:** hydroxyapatite, hydrothermal method, morphology, nanoparticles, experimental design

### Introduction

Hydroxyapatite ( $\text{Ca}_{10}(\text{PO}_4)_6(\text{OH})_2$ , HAp) nanoparticles, as one of the major components of hard tissues of the human body, are widely used in biomaterials because of their biocompatibility, bioactivity, low solubility in water and ability to replace toxic ions.<sup>1-10</sup> However, the low mechanical properties of HAp nanoparticles have limited their use in load-bearing orthopedic and dental applications.<sup>4,5</sup> Therefore, the synthesis of particles with optimized size, morphology, crystallinity, stoichiometry and phase composition has become a focus of interest in the biomedical fields.<sup>2-6</sup> In the literature, several methods for preparing HAp nanoparticles have been reported, including chemical precipitation,<sup>11,12</sup> solid-state synthesis,<sup>13,14</sup> sol-gel

process,<sup>11,15,16</sup> solvo-treatment process,<sup>17</sup> hydrothermal method,<sup>10,17-21</sup> biomimetic synthesis,<sup>22,23</sup> spray pyrolysis<sup>24,25</sup> and solvothermal procedure.<sup>26-28</sup> Moreover, many of such studies have been made to improve the mechanical properties, using one-dimensional growth of HAp crystals and preparing needle-like or rod-like particles.<sup>18-21,26-29</sup> It is known that HAp nanorods can be synthesized; however, the preparation of nano-sized particles with high aspect ratio, appropriate stoichiometry and high crystallinity still remains an important task.<sup>4,5,19-21,25-32</sup>

The hydrothermal method, which works at high temperature and high pressure, is the most frequently used technique for one-dimensional growth of HAp. This method enables the synthesis of HAp powders with high degree of crystallinity which are relatively stable in physiological medium.<sup>33</sup> The HAp prepared by this method is homogeneous and easily sinterable, with Ca/P

\*e-mail: m.shojai@ippi.ac.ir

molar ratios close to the stoichiometric value, owing to the effects of high temperature and high pressure on the aqueous solutions.<sup>4,10,17-27,34</sup> However, many different studies have resulted in discrepancies in the optimum experimental conditions. For instance, some works show that the rod-like HAp is synthesized in acidic<sup>5,35</sup> or approximately neutral conditions,<sup>28</sup> and others show that these nanorods are synthesized under alkaline conditions.<sup>30-32,36</sup> Moreover, only few experimental parameters were evaluated in each study.

The success of the hydrothermal procedure in the formation of HAp with high quality prompted us to investigate its capability to control the formation of HAp nanoparticles through an experimental design route. In the present study, we report the controlled growth of HAp nanoparticles with tunable size, morphology, crystallinity and stoichiometry by adjusting the experimental parameters under simple and relatively mild reaction conditions. Some of the synthesized HAp nanoparticles were of uniform shape and had high crystallinity with single phase; thus they are believed to be applicable for the preparation of various HAp bioceramics with improved mechanical properties.

## Experimental

### Materials

Calcium nitrate tetrahydrate as the calcium ion source, di-ammonium hydrogen phosphate as the phosphate

ion source, and ammonium solution (25%) and urea for adjusting pH were purchased from Merck (Germany) and used as received. All reagents were of analytical grade. Deionized water was used throughout all the experiments.

### Design of experiments (DOE)

Among the factors that may influence the characteristics of HAp, reaction temperature, pH, concentration of reactants and presence of urea were evaluated using a two-level random, full factorial experimental design approach. The response for the diameter, length, aspect ratio, crystallinity and stoichiometric ratio of the as-synthesized HAp was analyzed using the STATISTICA 6.0<sup>®</sup> software package. The time of hydrothermal treatment was kept constant at 60 h and other experimental domains were chosen using literature data.<sup>4,5,10,11,17,22,37-39</sup> Table 1 shows a 16-run experimental design with four variables and two levels utilized in the experiments, along with the codes for each sample (the words hydrothermal and urea are abbreviated as “Hy” and “U” in the sample codes, respectively). Each run was carried out independently, while the amount of independent variables varied according to the design.

The STATISTICA 6.0<sup>®</sup> software statistically analyzed the experimental data (*e.g.*, analysis of variance, ANOVA). The graphical display of data can be used to find a relationship between the input variables and the system responses. In

**Table 1.** Levels of factors and 2<sup>4</sup> experimental design matrix utilized in the synthesis of HAp nanoparticles

	Concentration of Reactants/(mol L <sup>-1</sup> )	pH	Urea	Temperature/(°C)
Low level (-1)	0.03	5.6	No	90
High level (+1)	0.1	10	Yes	200
Sample Codes	Design			
Hy5-90-0.03	-1	-1	-1	-1
Hy5-90-0.1	1	-1	-1	-1
Hy10-90-0.03	-1	1	-1	-1
Hy10-90-0.1	1	1	-1	-1
Hy-U-5-90-0.03	-1	-1	1	-1
Hy-U-5-90-0.1	1	-1	1	-1
Hy-U-10-90-0.03	-1	1	1	-1
Hy-U-10-90-0.1	1	1	1	-1
Hy5-200-0.03	-1	-1	-1	1
Hy5-200-0.1	1	-1	-1	1
Hy10-200-0.03	-1	1	-1	1
Hy10-200-0.1	1	1	-1	1
Hy-U-5-200-0.03	-1	-1	1	1
Hy-U-5-200-0.1	1	-1	1	1
Hy-U-10-200-0.03	-1	1	1	1
Hy-U-10-200-0.1	1	1	1	1

the present study, the effect of each factor was tested at the confidence limit of 95% (corresponding to a  $p$ -value of 0.05). The factors whose  $p$ -values were less than 0.05 were considered as “statistically significant”. A graphical display of the ordered standardized effect (estimated effect divided by its standard error) of each factor was given in a Pareto chart, which analyses the magnitude and the importance of each variable effect. The length of bars in the chart is proportional to the standardized effect. A factor was considered as “statistically significant” if its standardized effect exceeded a threshold. A line in the Pareto chart indicated the threshold for a test at the  $p$ -value of 0.05.

The mean for a given level of a variable is the average of all responses obtained for that level and used for plotting the marginal means. The plot of marginal means provides an important insight into the relationship between a quantitative response variable and the independent variables. Although the number that appears next to each horizontal bar in the Pareto charts shows that the parameter has a decreasing or increasing role, the plot of marginal means is interesting from an illustrative point of view. A plot for one independent variable (factor) with two levels can be obtained by placing the levels of that factor on the horizontal axis, and the total values of the dependent variable on the vertical axis. The final plot is then obtained by connecting the mean values of the dependent variable with two levels of the independent factor. The magnitudes of the variable effect can be determined from the slope of the line (the greater the degree of departure from horizontal, the stronger the effect). It shows whether the estimated marginal means are increasing or decreasing across the levels. It should be pointed out that in the present study the total calculations for plotting the Pareto chart as well as the plot of marginal means were automatically carried out using the STATISTICA® software package.

## Methods

First, solutions of the reacting ions (calcium and phosphate) with concentrations of 0.10 and 0.03 mol L<sup>-1</sup> respectively were prepared by dissolving the appropriate amount of the relevant salts in deionized water. The phosphate ion solution was then added dropwise into the calcium ion solution under continuous and gentle stirring, while the molar ratio (Ca/P) was kept at the stoichiometric amount according to its ratio in HAp (1.67). For the chemical precipitation experiments, which were performed under alkaline conditions (see Table 1), the pH of the mixture was adjusted to 10 by the addition of ammonia, and the final pH of the other suspensions was kept constant at 5.6.

The urea can be used in the precipitation reaction, leading to the further transformation to HAp due to the pH changes during urea hydrolysis. For this reason, urea was added into the same mixture (according to Table 1) at a concentration equal to that of the calcium ion at the beginning of the precipitation reactions and the solution was then stirred for 30 min to ensure that the urea dissolved completely. The HAp precursor suspension was transferred to a 100 mL autoclave (pressure vessel), and treated hydrothermally at 90 or 200 °C for 60 h (see Table 1). The final product was washed thoroughly (four times) with a mixture of deionized water and ethanol (volume ratio of 1:1), isolated by filtration after being centrifuged, dried at 60 °C and then crushed into powder form. The schematic flowchart for the preparation of HAp is illustrated in Figure 1.

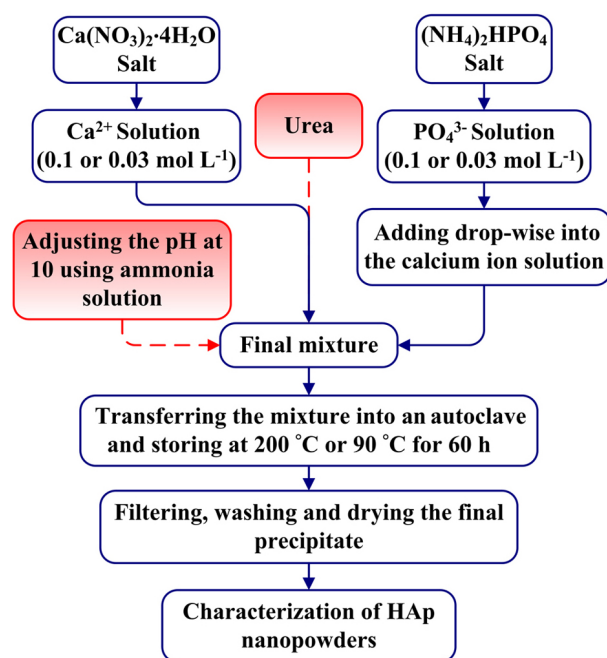


**Figure 1.** Flowchart for the synthesis of hydroxyapatite nanoparticles by the hydrothermal method.

The crystal and phase structures of the samples were identified using a X-ray diffractometer (XRD, Model D5000, Siemens Co.) with  $\text{CuK}\alpha$  ( $\lambda = 1.5418 \text{ \AA}$ ) incident radiation over the  $2\theta$  range of 20-60° at room temperature with a step size of 0.02°. The fraction of the crystalline phase ( $X_c$ ) in HAp nanoparticles was determined according to the following equation:<sup>40</sup>

$$X_c = 1 - (V_{112/300}/I_{300}),$$

where  $I_{300}$  represents the intensity of the (300) diffraction peak, and  $V_{112/300}$  represents the intensity of the valley

between the peaks of (112) and (300). Fourier transform infrared spectroscopy (FTIR, Model EQUINOX55, BRUKER, Germany) was used for identification of functional groups present in the HAp powder. Samples for FTIR analysis were prepared from 1:90 HAp-KBr mixtures (by weight), which were compacted into pellet form and then scanned from 4000 to 400  $\text{cm}^{-1}$ . The morphology and size of the nanoparticles were studied using scanning electron microscopy (SEM, Model VEGAII, XMU, TESCAN, Czech Republic) and transmission electron microscopy (TEM, Model CEM-902A, Zeiss Co, Germany, at an accelerating voltage of 80 kV). The elemental compositions of the products were quantitatively identified on an energy dispersive X-ray analyser (EDXA, Model QX2, RONTEC Co.) which was coupled to the SEM microscope.

## Results and Discussion

As mentioned in the experimental section, four factors were studied through an experimental design approach and the results of 16 experiments were subjected to the ANOVA process. In this process, the characteristics of the as-synthesized HAp were used as response functions, and the effects of the process variables on these characteristics were analyzed. Table 2 summarizes the characteristics of the as-synthesized HAp nanoparticles. The ranking of standardized effects of independent variables and possible cross effects for all responses are shown on the Pareto chart in Figure 2. The bars extending over the dotted vertical line

indicate that those effects are statistically significant at  $p = 0.05$ . Moreover, the plots of marginal means, resulting from the statistical analysis, are shown in Figure 3.

### Mean diameter of HAp nanoparticles

The diameter of the rod-like particles is of importance because it determines the surface area available for the matrix of a fiber-reinforced composite and, finally, its strength.<sup>7,41,42</sup> In general, the strength of a fiber decreases as its diameter increases.<sup>41,42</sup> Therefore, it is important to investigate the effects of different factors on the diameter of HAp nanoparticles. Figure 4 shows the overall morphology of the as-synthesized HAp nanoparticles and the average diameters of the samples are shown within parenthesis in the second column of Table 2. According to the table, the diameter of the particles varies from 35 to 320 nm for the samples Hy-U-10-90-0.1 and Hy-U-5-90-0.1 respectively. The ranking of standardized effects presented on the Pareto chart in Figure 2(a) indicates that none of the factors was statistically significant within the experimental range studied.

Figures 3(a-1), 3(b-1), 3(c-1) and 3(d-1) show respectively the marginal means plots of the effects of reactant concentration, pH, urea and temperature of hydrothermal treatment on the diameter of HAp nanoparticles. According to the Figure 3(a-1), the mean diameter of nanoparticles increases slightly with increasing the concentration of the chemical reactants. Considering the limitation of reaction time and higher numbers of ions *per*

**Table 2.** Results for diameter (D), length (L), aspect ratio (L/D), degree of crystallinity (%X<sub>c</sub>) and Ca/P ratio of the synthesized HAp nanoparticles

Sample Code	D (nm)	L (nm)	L/D	%X <sub>c</sub>	Ca/P
Hy5-90-0.03	60-80 (70)	200-450 (300)	4	29.7	1.62
Hy5-90-0.1	30-60 (40)	400-700 (450)	11	19.4	1.5
Hy10-90-0.03	20-50 (45)	20-50 (45)	1(spherical)	47.5	1.83
Hy10-90-0.1	55-85 (60)	55-85 (60)	1(spherical)	51.4	1.76
Hy-U-5-90-0.03	45-70 (55)	500-850 (600)	11	27.1	1.72
Hy-U-5-90-0.1	170-420 (320)	700-1300 (950)	3	40.4	1.66
Hy-U-10-90-0.03	35-70 (50)	35-70 (50)	1(spherical)	57.7	1.92
Hy-U-10-90-0.1	25-50 (35)	25-50 (35)	1(spherical)	48.3	1.86
Hy5-200-0.03	30-70 (50)	300-800 (450)	9	73.8	1.96
Hy5-200-0.1	30-95 (50)	850-1400 (1200)	24	73.1	1.69
Hy10-200-0.03	45-60 (50)	45-60 (50)	1(spherical)	70.7	1.7
Hy10-200-0.1	40-70 (50)	40-70 (50)	1(spherical)	61.2	1.88
Hy-U-5-200-0.03	65-80 (68)	250-400 (340)	5	75.1	1.89
Hy-U-5-200-0.1	30-70 (50)	450-900 (550)	11	83.8	1.79
Hy-U-10-200-0.03	45-60 (50)	45-60 (50)	1(spherical)	61.7	1.85
Hy-U-10-200-0.1	35-55 (40)	35-55 (40)	1(spherical)	64.5	1.82

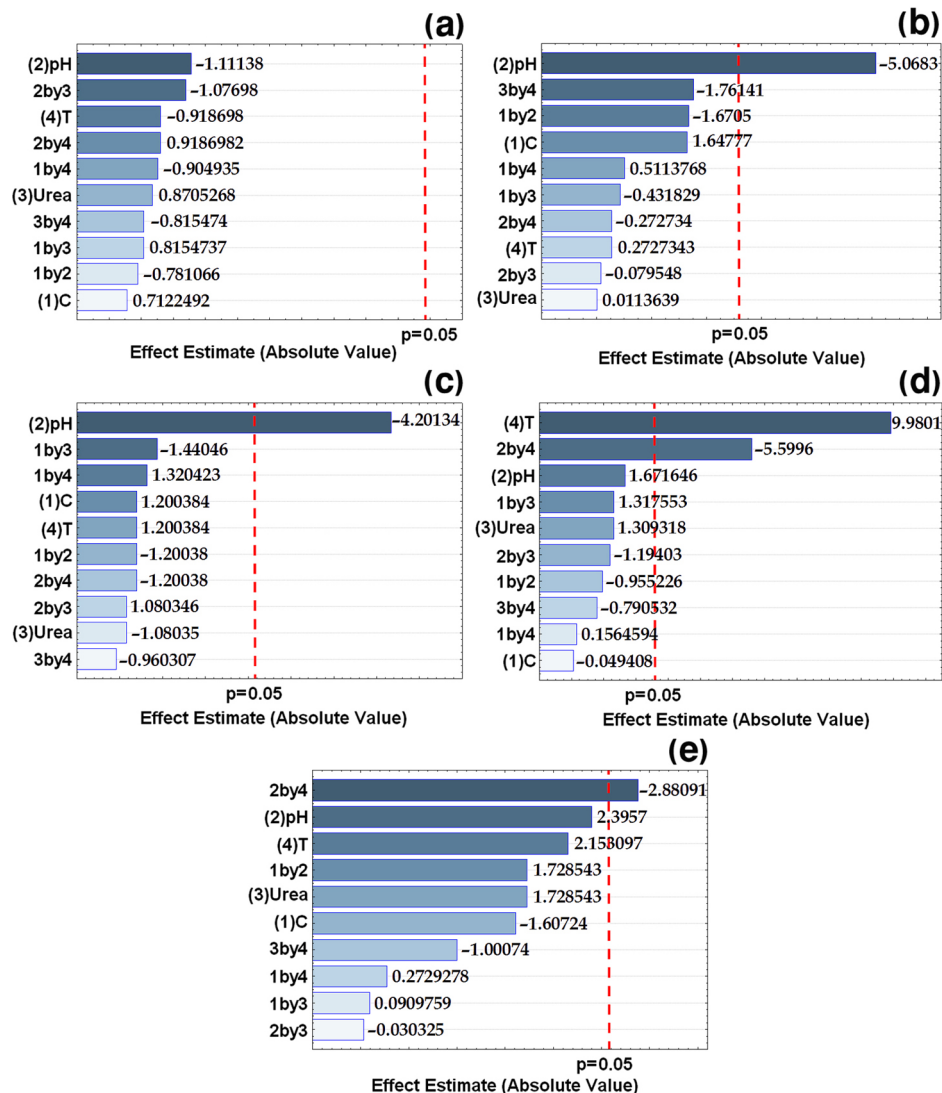


**Figure 2.** Pareto chart of standardized effects at the confidence limit of 95% for: (a) diameter, (b) length, (c) aspect ratio, (d) degree of crystallinity and (e) Ca/P ratio.

volume unit at higher reactants concentration, the higher diameter is therefore obtained at reactants concentration of  $0.1 \text{ mol L}^{-1}$ . In fact, there is general agreement that the growth rate of crystals in a less concentrated solution is too slow due to the ion transport control.

According to the Figure 3(b-1), the diameter of the nanoparticles decreases with increasing pH value. As shown in SEM images, under alkaline conditions the samples are formed in nearly spherical shape, suggesting that the crystal growth of HAp depends on the pH of the reaction mixture and that there is not any preference for an oriented crystal growth in alkaline conditions.

A modified method to synthesize HAp in basic conditions consisted of the addition of urea instead of ammonia in the precipitation reaction, which leads to more homogenous and biocompatible HAp and to further transformations due to the pH changes caused by urea

hydrolysis.<sup>23,35,43</sup> Moreover, during hydrolysis,  $\text{CO}_3^{2-}$  ions are released and incorporated into the crystal structure to produce carbonated hydroxyapatite.<sup>23,43</sup> For these reasons, urea was considered among the factors which may be important in the characteristics of the synthesized HAp. According to the results presented here (Figure 3(c-1)), the use of urea in the reaction medium increases the mean diameter of the nanoparticles. This can be related to the coordination of urea to  $\text{Ca}^{2+}$  ions in the starting mixture in which, by adjusting the  $\text{Ca}^{2+}$  ion release, the rate of formation of HAp is controlled.

It is suggested that the formation of HAp crystals through hydrothermal crystallization process includes two main stages, which can be schematically illustrated in Figure 5. The first stage is the nucleation (step of reaction of ions) and formation of tiny crystalline nuclei in a supersaturated medium, and the second is the growth of

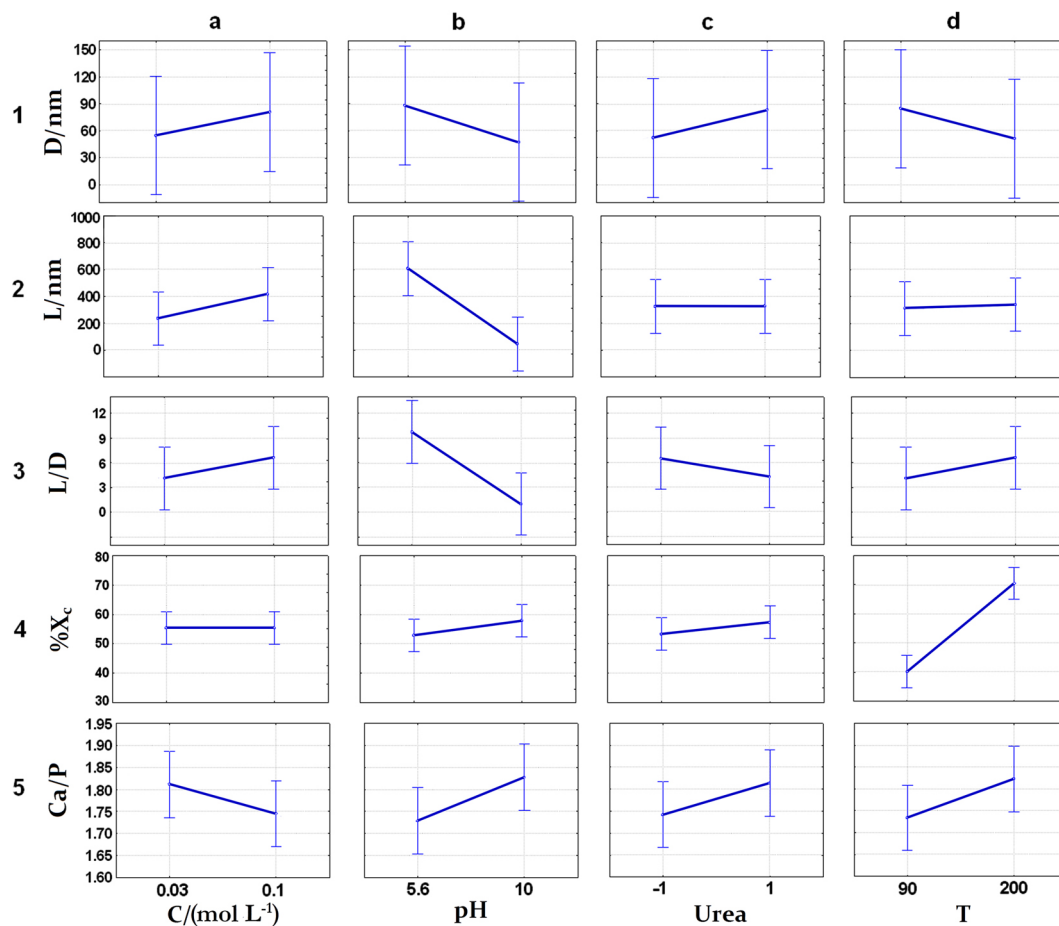


**Figure 3.** Plots of marginal means for diameter, length, aspect ratio, degree of crystallinity and Ca/P ratio.

the nuclei (step of hydrothermal treatment).<sup>2,19,20,44</sup> Due to the complete decomposition of urea at relatively elevated temperatures, urea can only affect the characteristics of HAp in the former stage. The complex urea-Ca<sup>2+</sup> prevents the Ca<sup>2+</sup> ions from reacting quickly with the other reactants and this, therefore, decreases the number of nucleation sites. Decreasing the number of nuclei allows them to increase in size, whereupon the diameter of nanoparticles increases. In other words, with the prolonged duration of the contact, the small crystallites are permitted to grow into larger particles. This is similar to the case described in a recent report in which ethylenediaminetetraacetic acid (EDTA) has been used as the chelating agent.<sup>45</sup>

Figure 3(d-1) shows that the mean diameter of nanoparticles slightly decreases with increasing temperature of the hydrothermal treatment. A comparison of this result with that in the following section reveals that the rod-like nanoparticles with high aspect ratio are synthesized from the precipitation reaction with higher hydrothermal temperature (an increase in mean length of nanorods is observed with increasing temperature during the hydrothermal treatment). These results show that the *c*-axis size increases when the

hydrothermal temperature increases, which is accompanied by decreasing in growth at the other directions.

#### *Mean length of rod-like HAp nanoparticles*

According to the Pareto chart presented in Figure 2(b), only the pH value of the reaction mixture has a significant effect on the mean length of the HAp nanorods. Moreover, reactants concentrations and interactions between the presence of urea and hydrothermal temperature (3 and 4), and between reactants concentrations and pH (1 and 2) are among the more influencing effects but are not statistically significant.

The marginal means plots of the effects of reactant concentration, pH, urea and temperature of hydrothermal treatment on the mean length of particles are respectively presented in Figures 3(a-2), 3(b-2), 3(c-2) and 3(d-2). Figure 3(a-2) indicates that the mean length of the nanoparticles increases as a response to the increasing concentration of the reactants, similar to the observed for the mean diameter of the nanoparticles. The explanation of this behavior may be similar to that given in the previous section.

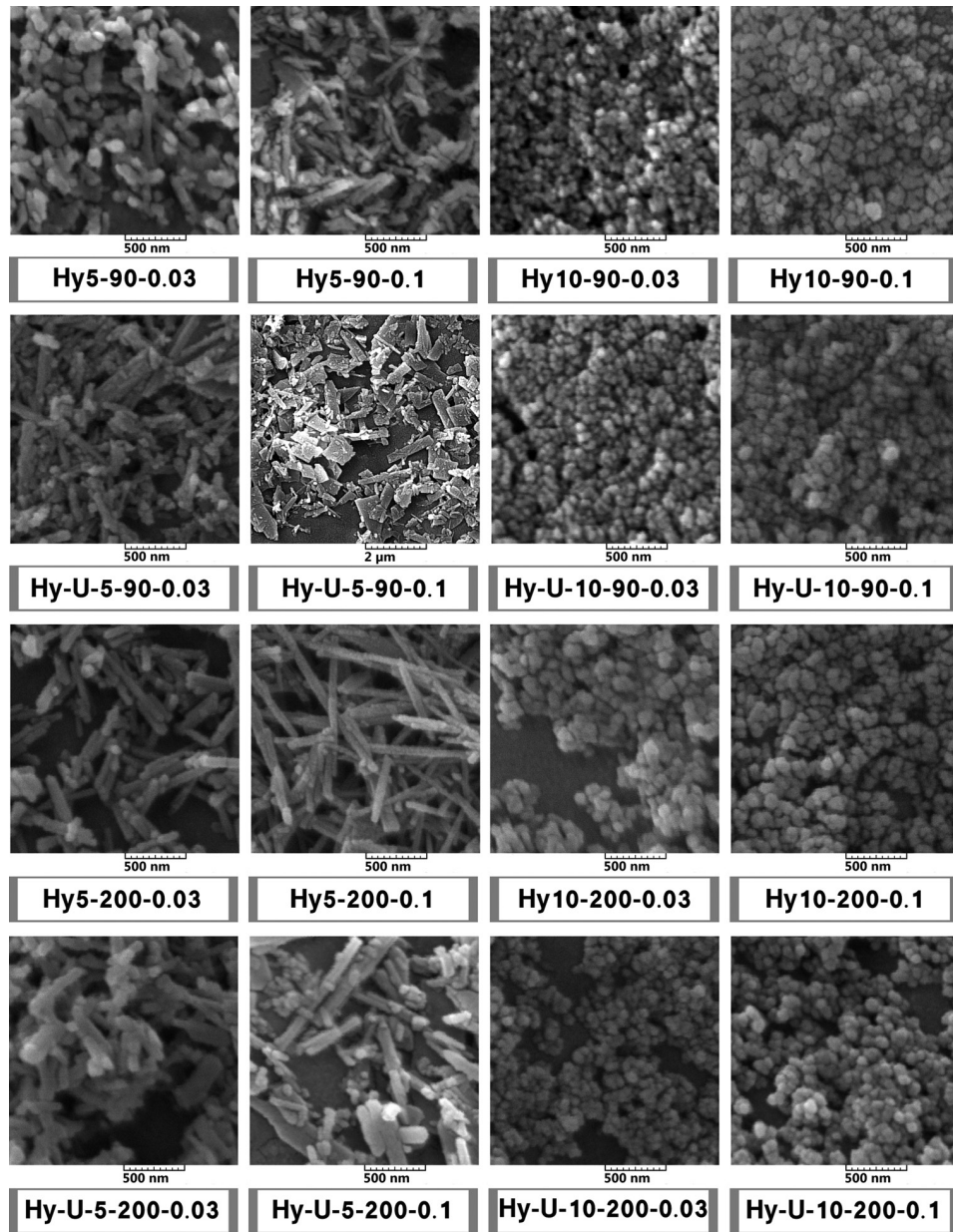


Figure 4. SEM images of the HAP nanoparticles.

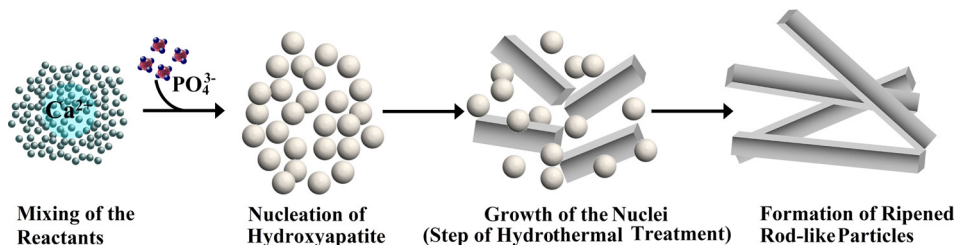


Figure 5. Preparation of rod-like HAP nanoparticles using the hydrothermal method.

Some previous studies have shown that the pH variation from basic to acidic conditions is favorable to the development of rod-like particles.<sup>5,29,35,46</sup> According to the present study (see Figure 3(b-2)), the mean length

of nanoparticles steeply decreases with increasing pH. In fact, the variation in pH has a pronounced influence on the length of the rod-like particles. This can be explained by the higher tendency of the nuclei to grow at the *c*-axis

in moderate acidic conditions. The results of the present study suggest that, at lower pH, calcium and phosphate ions preferentially adsorb on the particles at the *c*-axis, and the consequent unidirectional growth of the particles leads to the formation of nanorods. However, the effect of pH on the morphology of the HAp nanoparticles depends on the other factors, too. In fact, rod-like HAp can also be synthesized in basic conditions using alteration of the other parameters (for example, by use of surfactants or alteration of the temperature of preparation of the HAp precursor).

According to Figure 3(c-2), there is essentially no difference in the mean length of nanorods in the presence or absence of urea, within the experimental range studied. This result may be due to the decomposition of urea at higher temperatures, *i.e.*, in the stage of hydrothermal treatment, in which crystals grow. In contrast to urea, the Figure 3(d-2) indicates that the mean length of nanorods increases slightly with increasing hydrothermal temperature. This effect can be attributed to the tendency of the particles to grow in one direction at higher temperatures. Increasing temperature results in preferential crystal growth along the *c*-axis. However, this effect is found to be non-significant according to the Pareto chart in Figure 2(b).

#### Aspect ratio of rod-like HAp nanoparticles

In the previous sections, the effects of various factors on the diameter and length of the HAp nanoparticles were investigated. However, the net strength of a given rod-like particle is predominantly determined by its length to diameter ratio. It is well known that, for a given fiber, higher values of the length to diameter (or width) ratio, known as aspect ratio, result in improved strength of fiber-reinforced composites.<sup>41,42</sup> Calculated average aspect ratios for the samples are shown in Table 2, in which rod-like HAp particles with aspect ratios up to 24 can be seen. According to the Pareto chart shown in Figure 2(c), the pH has a significant effect on the aspect ratio of the nanorods.

Figures 3(a-3), 3(b-3), 3(c-3) and 3(d-3) show respectively the marginal means plots of the effects of reactant concentration, pH, urea and temperature of hydrothermal treatment on the aspect ratio of rod-like particles. As expected, this aspect ratio increases slightly as the concentration of reactants increases (Figure 3(a-3)). In fact, the increase in the mean length observed with increasing reactant concentration is larger than the increase in the mean diameter, whereupon the aspect ratio increases (see the numbers on the Pareto charts).

According to Figure 3(b-3), the aspect ratio steeply decreases with increasing pH of the reaction mixture. When applying basic conditions, a diminishing trend is seen in

both length and diameter. However, a comparison of the degree of departure from a horizontal line in Figure 3(b-1) with that in Figure 3(b-2) reveals that the aspect ratio must be decreasing steeply with increasing pH (see also the numbers on the Pareto charts). In fact, particles produced in basic conditions are actually spherical in shape.

Figure 3(c-3) indicates that the aspect ratio decreases slightly in the presence of urea. When urea is used in the reaction medium, the diameter of the particles increases (Figure 3(c-1)), while their mean length remains unchanged (Figure 3(c-2)), whereupon the aspect ratio decreases. Moreover, as a result of decreasing diameter and increasing length by increasing the hydrothermal temperature, the aspect ratio increases as the hydrothermal temperature increases (Figure 3(d-3)).

According to these results, rod-like HAp nanoparticles with high aspect ratio can be synthesized using high reactant concentrations at high hydrothermal temperature and low pH, without the use of urea in the reaction mixture. Figure 6 shows the large scale typical SEM and TEM micrographs of such HAp nanoparticles prepared under relatively optimum conditions.

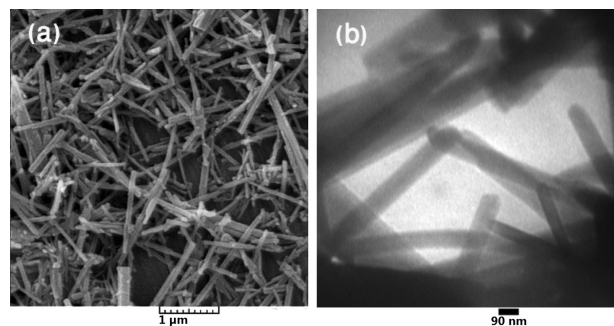


**Figure 6.** (a) SEM and (b) TEM images of the HAp nanorods corresponding to the sample Hy5-200-0.1.

#### The fraction of the crystalline phase in HAp nanoparticles

The XRD patterns of the HAp samples are presented in Figure 7 in the order of increasing degree of crystallinity.

All XRD patterns are identified as HAp according to the ICDD (International Centre for Diffraction Data) standard (PDF card no. 9-432) and all peaks correspond to the hexagonal crystal form of HAp.<sup>1,10,17,33,47-50</sup> From Figure 7, it can be seen that a decreasing degree of crystallinity leads to a decrease in intensity and an increase in width of the diffraction peaks. Moreover, the relative intensity of the peak (300) grows with the increase in the crystallinity degree, which shows that HAp may be oriented along the *c*-axis. The  $X_c$  values of the synthesized nanoparticles are shown in Table 2. It is well-known that the crystalline phase of HAp has an important contribution to the strength of the

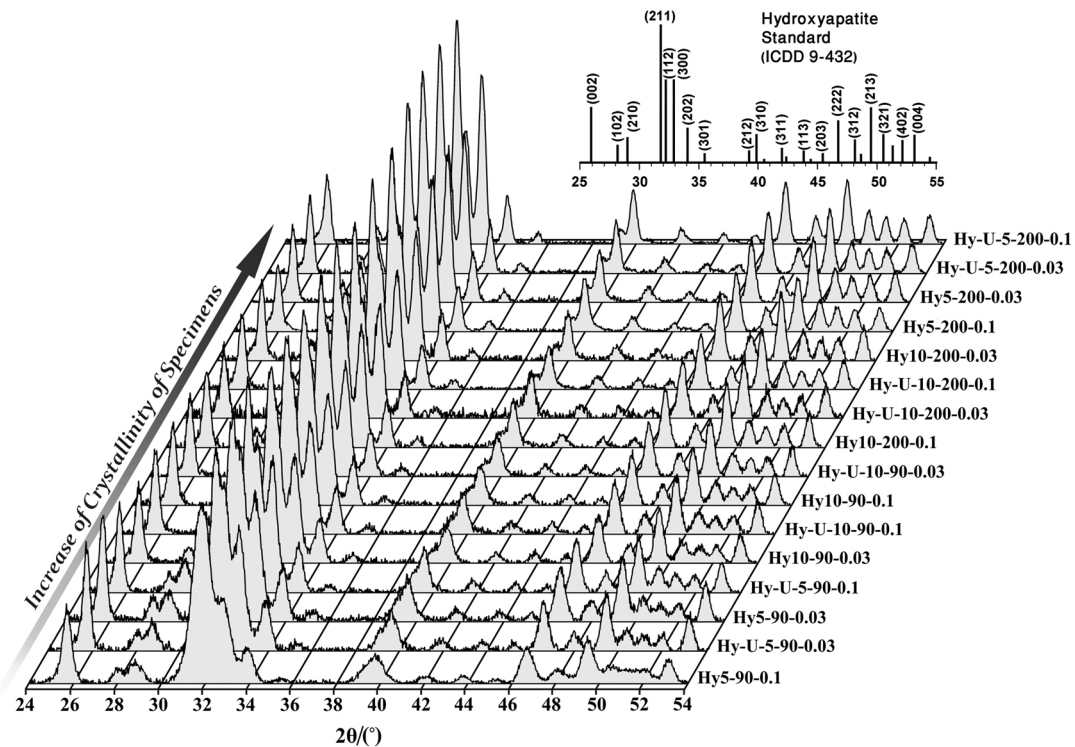


**Figure 7.** XRD patterns of HAp samples synthesized by the hydrothermal method together with the ICDD standard for HAp.

final ceramic or composite.<sup>24</sup> According to Table 2, various degrees of crystallinity from 19.4 to 83.8% can be obtained by design of experiments.

To confirm the HAp structure of samples, the IR spectra given in the supplementary material was used (Figure S1). The characteristic peaks for  $\text{PO}_4^{3-}$  appear at about 1090, 1029, 602, 961, 566 and 473  $\text{cm}^{-1}$ . The peaks at 3437 and 1637  $\text{cm}^{-1}$  are relative to the bending modes of the hydroxyl group in the adsorbed water, while the peaks at 3571 and 633  $\text{cm}^{-1}$  are assigned to the stretching vibration of the hydroxyl group in the crystalline structure of HAp.<sup>33,35,40,50-57</sup> From Figure S1, it can be seen that, with decreasing degree of crystallinity, the intensity of the absorption bands appearing at 3437 and 1637  $\text{cm}^{-1}$  increases, while the intensity of the bands at 3571 and 633  $\text{cm}^{-1}$  decreases. Therefore, according to the results presented here, the change in the intensity of the aforementioned peaks could be used as an alternative to the XRD patterns for determination of the degree of crystallinity. Moreover, the weak peaks at 1400-1600  $\text{cm}^{-1}$ , associated with the carbonate  $\nu_3$  absorption band, indicate the presence of low amounts of carbonate impurities in the structure of HAp.<sup>53-61</sup> According to the IR spectra, the intensity of these peaks increased as the crystalline fraction decreased. Therefore, the presence of carbonate in the apatite lattice causes a decrease in crystallinity. Meanwhile the weak peak at about 873  $\text{cm}^{-1}$  may be attributed to the carbonate groups

or low amount of hydrogen phosphate in the crystalline structure of HAp.<sup>53-55</sup> Further analysis of the IR spectra in the region of 1400-1600  $\text{cm}^{-1}$  provided information on the sites in which the carbonate groups were substituted. Although the published data in the literature has led to some contradictory explanations regarding which bands correspond to the A-type (carbonate replacing  $\text{OH}^-$  ions), B-type (carbonate replacing  $\text{PO}_4^{3-}$  ions), or mixed AB-type carbonate substitution, the results of IR analysis in recent studies<sup>53-55,58-60</sup> indicate that the nanoparticles synthesized in the present work correspond mostly to a mixed AB-type substitutions of  $\text{CO}_3^{2-}$  in the hydroxyapatite lattice along with the predominance of B-type substitution.

From the viewpoint of crystal growth, each factor that diminishes the reaction rate of calcium and phosphate ions in the precursor preparation step or accelerates the growth of the nuclei in the hydrothermal treatment step causes an increase in the crystalline fraction of HAp nanoparticles. The ranking of standardized effects on the fraction of the crystalline phase is shown on the Pareto chart in Figure 2(d). According to the diagram, the hydrothermal temperature and the interaction between temperature and pH (2 by 4) have significant effects on the degree of crystallinity.

The marginal means plots of the effects of reactant concentration, pH, urea and temperature of hydrothermal treatment on the degree of crystallinity are respectively shown in Figures 3(a-4), 3(b-4), 3(c-4) and 3(d-4).

According to the Figure 3(a-4), there is no significant difference in the fraction of the crystalline phase in HAPs prepared at different reactant concentrations, within the experimental range studied. This could be explained by the fact that the change in the reactant concentration can not affect the growth rate of the nuclei at the step of hydrothermal treatment. However, according to the Figure 3(b-4), the crystallinity degree of HAP particles can increase slightly with increasing pH of the reaction mixture. This increase in the degree of crystallinity can be attributed to the suppression of the competing phosphate hydrolysis reaction. In fact, in basic conditions and elevated temperature (90 or 200 °C), the concentration of  $\text{PO}_4^{3-}$  (in comparison with  $\text{HPO}_4^{2-}$  as well as  $\text{H}_2\text{PO}_4^-$ ) is much higher, which may cause an increase in the rate of nucleation. Therefore, the results of the experiments and statistical analysis reported here revealed that the pH value effectively controls the particle size and crystallinity degree, together with other properties of the HAP nanoparticles.

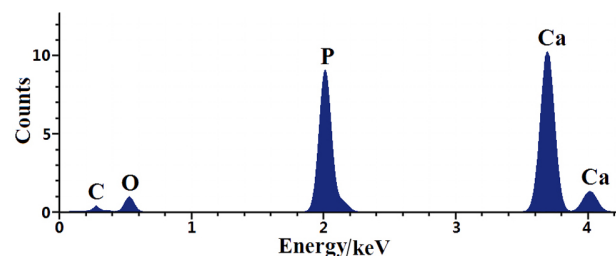
Figure 3(c-4) shows that urea increases the crystalline fraction of the HAP nanoparticles. This could be explained by the coordination of calcium ions to the urea molecules to form a  $\text{Ca}^{2+}$ -urea complex in the starting reaction mixture. This complex can effectively control the growth of HAP at the precursor preparation step by decreasing the  $\text{Ca}^{2+}$  ion release, whereupon the degree of crystallinity of nanoparticles increases. In other words, with the prolonged duration of the reaction between ionic reactants, the small crystallites are allowed to grow and increase the crystalline fraction in HAP particles.

Figure 3(d-4) indicates that the degree of crystallinity steeply increases with increasing hydrothermal temperature. According to the figure, in order to obtain highly crystalline HAP nanoparticles, it is necessary to work at high temperatures. This can be explained by the higher susceptibility of nuclei to grow at higher temperatures, which may be a consequence of the orientation along the plane (300).

#### The Ca/P ratio of HAP nanoparticles

The Ca/P ratio in HAP nanoparticles is determined as a measure of their stoichiometry.<sup>2,4,33,50</sup> The measurement of this ratio can be performed with energy dispersive X-ray analysis (EDXA).<sup>2,33,50,62</sup> Figure 8 shows a typical EDXA spectrum of the prepared HAP nanoparticles. The calculated Ca/P ratios of HAP samples are presented in Table 2. Stoichiometric products have a Ca/P ratio of 1.67, but powders obtained by wet methods are usually non-stoichiometric. Moreover, the presence of a carbon

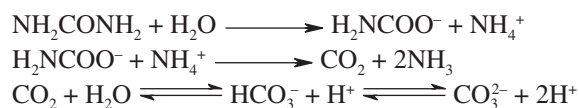
peak at 0.23 keV in the EDXA spectra provides further evidence for the presence of the carbonate group in the crystal structure of non-stoichiometric samples. Figure 2(e) shows the Pareto chart for the Ca/P ratio resulting from the statistical analysis. According to the diagram, the absolute effects of all variables under consideration on the Ca/P ratio are not significant. However, the interaction between hydrothermal temperature and pH was found to be statistically significant.



**Figure 8.** Typical EDXA spectrum of the HAP nanoparticles corresponding to the sample Hy5-200-0.1.

Figures 3(a-5), 3(b-5), 3(c-5), and 3(d-5) show respectively the marginal means plots of the effects of reactant concentration, pH, urea and temperature of hydrothermal treatment on the Ca/P ratio of HAP nanoparticles. Figure 3(a-5) indicates that the Ca/P ratio of nanoparticles decreases slightly with increasing concentration of the chemical reactants. The results show that the crystal growth of HAP in a highly concentrated solution proceeds through the formation of a precursor with a Ca/P molar ratio smaller than the stoichiometric value. However, this effect is not statistically significant.

According to the Figures 3(b-5), 3(c-5) and 3(d-5), the Ca/P ratio of HAP nanoparticles increases by increasing the pH, using urea or increasing the temperature of the hydrothermal treatment. In fact, the possibility of absorption of  $\text{CO}_2$  from the air during the reaction in basic media is much higher, resulting in the higher concentration of  $\text{CO}_3^{2-}$  in the reaction mixture. On the other hand, with increasing temperature, urea decomposes completely and produces carbon dioxide. The decomposition of urea and production of carbonate ions in aqueous solutions can be described by the following reactions:<sup>63</sup>



At constant calcium content, by increasing the carbonate concentration in the reaction mixture, the absorption of the phosphate ions is suppressed and therefore the Ca/P ratio increases.

## Conclusions

We developed a general methodology to predict the suitable conditions for the hydrothermal synthesis of HAp nanoparticles. The process variables that may influence the characteristics of HAp nanoparticles, including reactants concentration, pH, temperature of the hydrothermal treatment and presence of urea in the reaction medium, were studied through an experimental design route. The products were characterized and the results for different responses, including diameter, length, aspect ratio, degree of crystallinity and Ca/P ratio were subjected to the ANOVA analysis. Among the selected variables, temperature and pH were found to be the most significant parameters affecting the HAp structural and morphological properties. It was shown that both the length and the aspect ratio of HAp particles were significantly affected by the pH of the reaction mixture. Moreover, it was shown that the temperature of hydrothermal treatment and an interaction between pH and the aforementioned temperature significantly influenced the degree of crystallinity of the products. It was also found that the Ca/P ratio was significantly affected by an interaction between pH and temperature. Meanwhile, urea appeared to be a controller for crystal formation and affected the chemical composition, crystal morphology and particle size during the preparation. This is the first report of a systematic evaluation of the most influencing variables in the synthesis of HAp by the hydrothermal method, and of their effects on the HAp properties. The methodology can probably be extended to other methods of synthesis of HAp and thus can be used to prepare a wide range of HAp particles with very different physical and chemical properties, which have potential application in preparing various types of biomaterials.

## Supplementary Information

Supplementary information (FTIR Spectra of six HAp samples) is available at <http://jbcs.sbg.org.br>, as PDF file free of charge.

## References

- Zhang, Y.; Zhou, L.; Li, D.; Xue, N.; Xu, X.; Li, J.; *Chem. Phys. Lett.* **2003**, 376, 493.
- Zhang, F.; Zhou, Z.-H.; Yang, S.-P.; Mao, L.-H.; Chen, H.-M.; Yu, X.-B.; *Mater. Lett.* **2005**, 59, 1422.
- Zhang, Y.; Yokogawa, Y.; Feng, X.; Tao, Y.; Li, Y.; *Ceram. Int.* **2010**, 36, 107.
- Lin, K.; Chang, J.; Cheng, R.; Ruan, M.; *Mater. Lett.* **2007**, 61, 1683.
- Earl, J. S.; Wood, D. J.; Milne, S. J.; *J. Phys.: Conf. Ser.* **2006**, 26, 268.
- Sinha, A.; Nayar, S.; Kar, A.; Gunjan, M. K.; Mahato, B.; Das, G.; Kumar, A.; Chabra, A.; *Int. J. Appl. Ceram. Technol.* **2008**, 5, 458.
- Yi, Z.; Yubao, L.; Jidong, L.; Xiang, Z.; Hongbing, L.; Yuanyuan, W.; Weihu, Y.; *Mater. Sci. Eng., A* **2007**, 452, 512.
- Wang, X.; Li, Y.; Wei, J.; De Groot, K.; *Biomaterials* **2002**, 23, 4787.
- Chen, D. Z.; Tang, C. Y.; Chan, K. C.; Tsui, C. P.; Yu, P. H. F.; Leung, M. C. P.; Uskokovic, P. S.; *Compos. Sci. Technol.* **2007**, 67, 1617.
- Sadat-Shojai, M.; Atai, M.; Nodehi, A.; Nasiri Khanlar, L.; *Dent. Mater.* **2010**, 26, 471.
- Guzman Vazquez, C.; Pina Barba, C.; Munguia, N.; *Rev. Mex. Fis.* **2005**, 51, 284.
- Shi, H.-B.; Zhong, H.; Liu, Y.; Gu, J.-Y.; Yang, C.-S.; *Key Eng. Mater.* **2007**, 330, 271.
- Pramanik, S.; Agarwal, A. K.; Rai, K. N.; Garg, A.; *Ceram. Int.* **2007**, 33, 419.
- Cuneyt Tas, A.; *J. Am. Ceram. Soc.* **2001**, 84, 295.
- Bose, S.; Saha, S. K.; *J. Am. Ceram. Soc.* **2003**, 86, 1055.
- Zhang, S.; Wang, Y. S.; Zeng, X. T.; Cheng, K.; Qian, M.; Sun, D. E.; Weng, W. J.; Chia, W. Y.; *Eng. Fract. Mech.* **2007**, 74, 1884.
- Sadat-Shojai, M.; *J. Iran. Chem. Soc.* **2009**, 6, 386.
- Niu, J. L.; *Key Eng. Mater.* **2007**, 330, 247.
- Zhang, X.; Vecchio, K. S.; *J. Cryst. Growth* **2007**, 308, 133.
- Ashok, M.; Kalkura, S. N.; Sundaram, N. M.; Arivuoli, D.; *J. Mater. Sci.: Mater. Med.* **2007**, 18, 895.
- Komarneni, S.; Katsuki, H.; *Pure Appl. Chem.* **2002**, 74, 1537.
- Bayraktar, D.; Tas, A. C.; *Turk. J. Med. Sci.* **2000**, 30, 235.
- Bayraktar, D.; Tas, A. C.; *J. Eur. Ceram. Soc.* **1999**, 19, 2573.
- An, G.-H.; Wang, H.-J.; Kim, B.-H.; Jeong, Y.-G.; Choa, Y.-H.; *Mater. Sci. Eng., A* **2007**, 449, 821.
- Cho, J. S.; Kang, Y. C.; *J. Alloys Compd.* **2009**, 464, 282.
- Wang, Y. J.; Lai, C.; Wei, K.; Chen, X.; Ding, Y.; Wang, Z. L.; *Nanotechnology* **2006**, 17, 4405.
- Guo, X.; Xiao, P.; *J. Eur. Ceram. Soc.* **2006**, 26, 3383.
- Sun, Y.; Guo, G.; Tao, D.; Wang, Z.; *J. Phys. Chem. Solids* **2007**, 68, 373.
- Liu, Y.; Hou, D.; Wang, G.; *Mater. Chem. Phys.* **2004**, 86, 69.
- Liu, J.; Ye, X.; Wang, H.; Zhu, M.; Wang, B.; Yan, H.; *Ceram. Int.* **2003**, 29, 629.
- Zhu, R.; Yu, R.; Yao, J.; Wang, D.; Ke, J.; *J. Alloys Compd.* **2008**, 457, 555.
- Jiang, D.; Zhang, J.; *Curr. Appl. Phys.* **2009**, 9, S252.
- Felício-Fernandes, G.; Laranjeira, M. C. M.; *Quim. Nova* **2000**, 23, 441.
- Murugan, R.; Ramakrishna, S.; *Am. J. Biochem. Biotechnol.* **2007**, 3, 118.

35. Zhang, H.; Yan, Y.; Wang, Y.; Li, S.; *Mater. Res.* **2003**, *6*, 111.
36. Liu, C.; Huang, Y.; Shen, W.; Cui, J.; *Biomaterials* **2001**, *22*, 301.
37. Wang, A.; Yin, H.; Liu, D.; Wu, H.; Wada, Y.; Ren, M.; Xu, Y.; Jiang, T.; Cheng, X.; *Appl. Surf. Sci.* **2007**, *253*, 3311.
38. Sadat-Shojai, M.; *Hydroxyapatite: Inorganic Nanoparticles of Bone (Properties, Applications, and Preparation Methodologies)*, Iranian Students Book Agency (ISBA): Tehran, 2010 (in Persian).
39. Sadat-Shojai, M.; Atai, M.; Nodehi, A.; *Abstracts of the 9<sup>th</sup> International Seminar on Polymer Science and Technology*, Tehran, Iran, 2009.
40. Pang, Y. X.; Bao, X.; *J. Eur. Ceram. Soc.* **2003**, *23*, 1697.
41. Vasiliev, V. V.; Morozov, E.; *Mechanics and Analysis of Composite Materials*, Elsevier: London, 2001.
42. Kim, J.-K.; Mai, Y.-W.; *Engineered Interfaces in Fiber Reinforced Composites*, Elsevier: Netherlands, 1998.
43. Janackovic, Dj.; Jankovic-Castvan, I.; Petrovic, R.; Kostic-Gvozdenovic, Lj.; S. Milonjic, K.; Uskokovic, D.; *Key Eng. Mater.* **2003**, *240*, 437.
44. Di Chen, J.; Wang, Y. J.; Wei, K.; Zhang, S. H.; Shi, X. T.; *Biomaterials* **2007**, *28*, 2275.
45. Chen, H.; Sun, K.; Tang, Z.; Law, R. V.; Mansfield, J. F.; Czajka-Jakubowska, A.; Clarkson, B. H.; *Cryst. Growth Des.* **2006**, *6*, 1504.
46. Guo, G.-S.; Sun, Y.-X.; Wang, Z.-H.; Guo, H.-Y.; *Xiandai Huagong (Mod. Chem. Ind.)* **2004**, *24*, 43.
47. Shanthi, P. M. S.; Ashok, M.; Balasubramanian, T.; Riyasdeen, A.; Akbarsha, M. A.; *Mater. Lett.* **2009**, *63*, 2123.
48. Suvorova, E. I.; Buffat, P. A.; *Eur. Cell. Mater.* **2001**, *1*, 27.
49. Ha, J.-S.; *J. Korean Ceram. Soc.* **2003**, *40*, 1154.
50. Zhang, H.-B.; Zhou, K.-C.; Li, Z.-Y.; Huang, S.-P.; *J. Phys. Chem. Solids* **2009**, *70*, 243.
51. Sun, Y.; Guo, G.; Wang, Z.; Guo, H.; *Ceram. Int.* **2006**, *32*, 951.
52. Chen, H.; Clarkson, B. H.; Sun, K.; Mansfield, J. F.; *J. Colloid Interface Sci.* **2005**, *288*, 97.
53. Koutsopoulos, S.; *J. Biomed. Mater. Res.* **2002**, *62*, 600.
54. Lafon, J. P.; Champion, E.; Bernache-Assollant, D.; *J. Eur. Ceram. Soc.* **2008**, *28*, 139.
55. Chow, L. C.; Sun, L.; Hockey, B.; *J. Res. Natl. Inst. Stand. Technol.* **2004**, *109*, 543.
56. Landi, E.; Celotti, G.; Logroscino, G.; Tampieri, A.; *J. Eur. Ceram. Soc.* **2003**, *23*, 2931.
57. Bonfield, W.; Gibson, I. R.; *US Pat. 6,582,672*, **2003**.
58. Kumar, R.; Prakash, K. H.; Cheang, P.; Khor, K. A.; *Langmuir* **2004**, *20*, 5196.
59. Zhang, Z. H.; Huang, Z. L.; Shi, H. B.; Chi, R. A.; Li, J. Q.; Sun, N.; *J. Alloys Compd.* **2009**, *486*, 415.
60. Robinson, J. H.; Best, S. M.; *Key Eng. Mater.* **2009**, *396*, 649.
61. Gibson, I. R.; Bonfield, W.; *J. Biomed. Mater. Res.* **2002**, *59*, 697.
62. Cengiz, B.; Gokce, Y.; Yildiz, N.; Aktas, Z.; Calimli, A.; *Colloid Surface A* **2008**, *322*, 29.
63. Rahimpoure, M. R.; *Chem. Eng. Process.* **2004**, *43*, 1299.

Submitted: May 6, 2010

Published online: November 23, 2010

# Supplementary Information

## Design of Experiments (DOE) for the Optimization of Hydrothermal Synthesis of Hydroxyapatite Nanoparticles

Mehdi Sadat-Shojai,\* Mohammad Atai and Azizollah Nodehi

Iran Polymer and Petrochemical Institute, P.O. Box 14965-115 Tehran, Iran

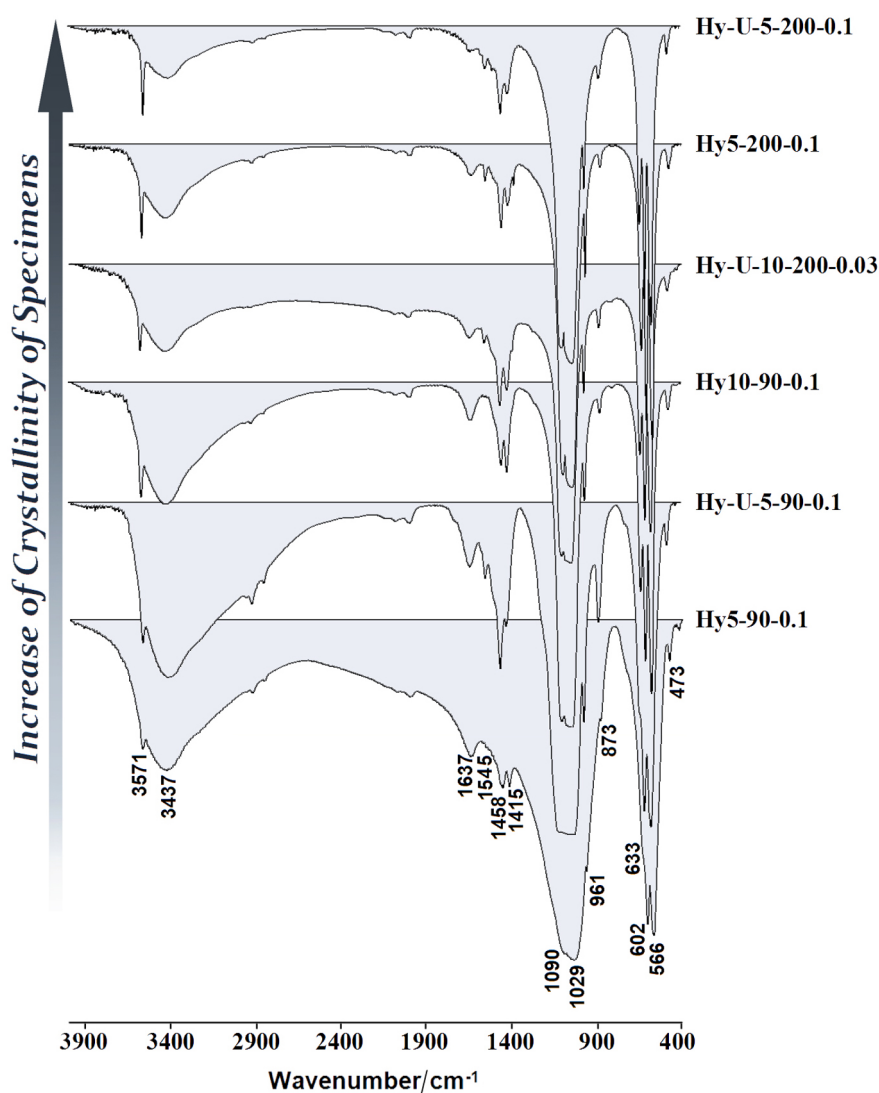


Figure S1. FTIR spectra of HAp samples (for clarity, only six spectra were shown).

\*e-mail: M.Shojai@ippi.ac.ir